# Meteorological predictions for the Beagle 2 mission to Mars

Scot C. Randell Rafkin,[1] Timothy I. Michaels,[1] and Robert M. Haberle[2]

[1]   A general circulation and mesoscale model are used to predict the weather at the Beagle 2 landing site. The afternoon high temperature predicted by the general circulation model varies from 237 to 243 K over the duration of the primary mission. The overnight low temperature is 193 K $\pm$ 2 K. Near surface wind speeds remain below 15 ms$^{-1}$ at all times. The mesoscale model predicts a wind maximum at the top of the $\sim$4 km deep convective boundary layer. Gravity waves are evident in the free atmosphere above the PBL. The overall weather pattern is dominated by upslope and downslope circulations, but these are modulated by changes in the large-scale circulation.   *INDEX TERMS:* 0343 Atmospheric Composition and Structure: Planetary atmospheres (5405, 5407, 5409, 5704, 5705, 5707); 6225 Planetology: Solar System Objects: Mars; 5445 Planetology: Solid Surface Planets: Meteorology (3346); 3346 Meteorology and Atmospheric Dynamics: Planetary meteorology (5445, 5739); 3329 Meteorology and Atmospheric Dynamics: Mesoscale meteorology. **Citation:** Rafkin, S. C. R., T. I. Michaels, and R. M. Haberle (2004), Meteorological predictions for the Beagle 2 mission to Mars, *Geophys. Res. Lett.*, *31*, L01703, doi:10.1029/2003GL018966.

## 1. Introduction

[2]   We present the meteorological environment of the Beagle 2 mission as predicted by the NASA Ames Mars General Circulation Model (MGCM) [*Haberle et al.*, 1997] and by the Mars Regional Atmospheric Modeling System (MRAMS) [*Rafkin et al.*, 2001]. The landing site is within an ellipse centered in Isidis Planitia at 11.6°N, 90.738°E. Entry, descent, and landing (EDL) will take place in the mid-afternoon at $L_s \approx 322$.

[3]   The weather at the landing site affects EDL operations. The diurnal variation of temperature will impact power consumption. The air bag landing system is sensitive to low level wind and wind shear [*Bridges et al.*, 2003].

[4]   MGCM results are used to characterize the large-scale atmospheric fields over the primary mission (approximately 180 sols; to $L_s \approx 51$). MGCM output is also used as initial and boundary conditions for the mesoscale MRAMS simulations. Two MRAMS simulations covering roughly four sols each are conducted for the start and end of the mission.

[5]   Atmospheric mesoscale modeling studies from MRAMS and MM5 were used during the selection process for the Mars Exploration Rovers [*Rafkin and Michaels*, 2003; *Toigo et al.*, 2004; *Kass et al.*, 2003]. Unfortunately, MER carries no meteorological instruments, and will effectively provide no data beyond atmospheric structure retrievals from the accelerometer during EDL. Hence, there will be no way to critically evaluate model performance. Beagle 2 carries a suite of meteorological instruments that will permit the validation of model results (Table 1). All the models have demonstrated skill at the three previous Mars lander sites: VL1, VL2, and Pathfinder [*Rafkin et al.*, 2001; *Toigo and Richardson*, 2002; *Tyler et al.*, 2002].

## 2. Model Configuration

[6]   The last year of a two year MGCM simulation is utilized for analysis. The MGCM grid spacing is 7.5° latitude by 9.0° longitude with 30 vertical layers. The lowest vertical level is a few meters above the ground. The global dust opacity is fixed at 0.45 at the 611 Pa level with a Conrath-$\nu$ value of 0.03. MRAMS was configured with six nested grids beginning with a horizontal spacing of 240 km and ending at approximately 550 m on the first and sixth grid, respectively. The simulation at the end of the mission used only five nested grids down to a spacing of 1.67 km. The fifth grid is designed to completely encompass the 174 km $\times$ 106 km east-west oriented landing ellipse. There are 60 vertical levels that are gradually stretched from 15 m to a spacing no more than 2 km. The model top is at approximately 50 km. Each simulation is approximately four sols in duration.

## 3. Results

### 3.1. Near-Surface Meteorology Over Duration of Mission

[7]   MGCM data for the length of the mission are shown in Figure 1. Pressure has a long-term seasonal cycle and a daily cycle associated with tides. The seasonal cycle reflects the growth of the northern polar cap for approximately the first 60 sols, followed by the sublimation of the cap during the northern hemisphere spring. There are pronounced peaks and troughs associated with the diurnal and semi-diurnal tides.

[8]   The mean wind speed does not vary significantly over the duration of the mission. The variance of the wind speed is reduced slightly from sols 100 to 140. Peak winds never exceed 15 ms$^{-1}$.

[9]   The temperature cycle is highly repeatable. The maximum temperature ranges from 237 K to 243 K during the primary mission with a $\pm$2 K variation from sol to sol. Temperature minima range from 192 K to 194 K.

### 3.2. Mesoscale Meteorology at Start and end of Primary Mission
#### 3.2.1. Time Series

[10]   Time series of temperature, pressure and winds predicted by MRAMS for the first and last few sols of the

---

[1]Department of Space Studies, Southwest Research Institute®, Boulder, Colorado, USA.
[2]Space Science Division, NASA Ames Research Center, Moffet Field, California, USA.

**Table 1.** Beagle 2 Meteorological Sensors

| Variable | Instrument Specifications |
|---|---|
| air temperature | 73K to 323K ± 0.1K |
| pressure | 0Pa to 3000Pa ± 0.4 Pa |
| wind speed | 0 to 80 m/s ± 0.1 m/s |
| wind direction | ±3° |

Nominal data sampling is O(10 minutes), but high frequency sampling of O(1 Hz) is possible. Temperature and wind sensors are on moveable robotic arm. Temperature is also taken at 10 cm above ground.
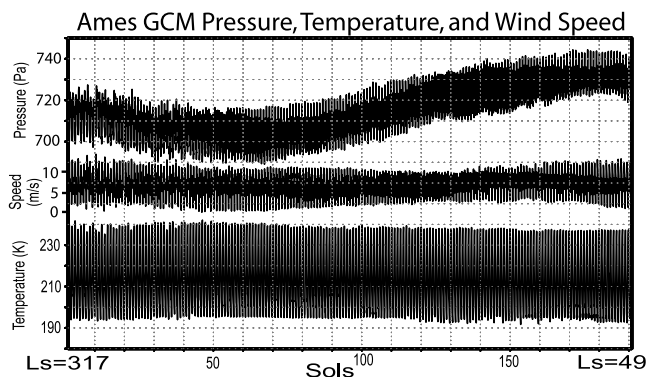
mission are shown in Figure 2. Note that time is given in Mars Universal Time, which is the local solar time at the 0° meridian. Add six hours to convert to lander time. The temperature data are reduced to 2 m while the other parameters are taken from the lowest level (∼15 m). The different mean pressure in Figures 1 and 2 is due primarily to the more accurate representation of landing site elevation by the mesoscale model (MOLA and MRAMS: −3750 m, MGCM: −3200 m).

[11] The variation of meteorological parameters at the start and end of the mission are similar. The most obvious differences are the amplification of the local pressure minima at 1800, and a slight phase shift in the temperature and pressure signals. The maximum temperature is lower at the end of the mission. This appears to result from the higher pressure and therefore greater thermal mass, and an increase in dust optical depth at the end of the mission.
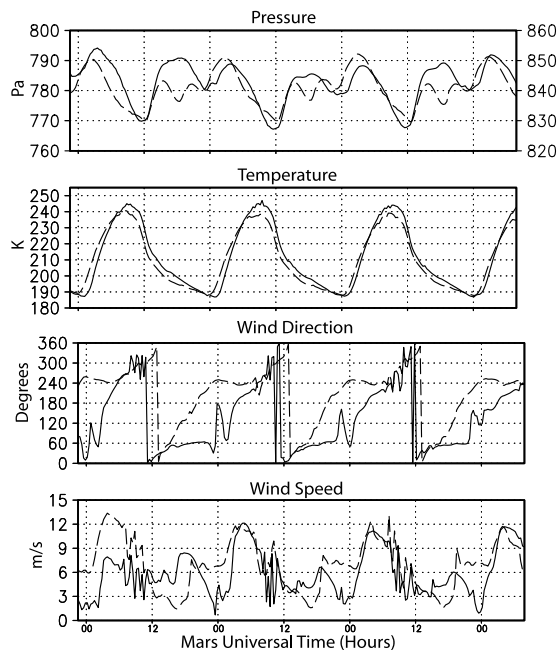
[12] The winds rotate clockwise with time, completing one revolution each sol. The differences between the two MRAMS simulations are attributed to differences in the large-scale mean wind in the region, as discussed in Section 3.2.4.

### 3.2.2. Vertical Profiles During EDL

[13] Vertical profiles of temperature, wind speed, vertical wind speed, and subgrid-scale turbulent kinetic energy (TKE) are shown in Figure 3. TKE is a measure of the kinetic energy within atmospheric circulations that are too small to be resolved by the model. They can be thought of as the "gustiness" of the wind. The profiles are deceiving as they represent only snapshots in a highly structured and rapidly evolving convective planetary boundary layer (PBL). There is a significant time-varying component, particularly to the profiles of vertical velocity and wind
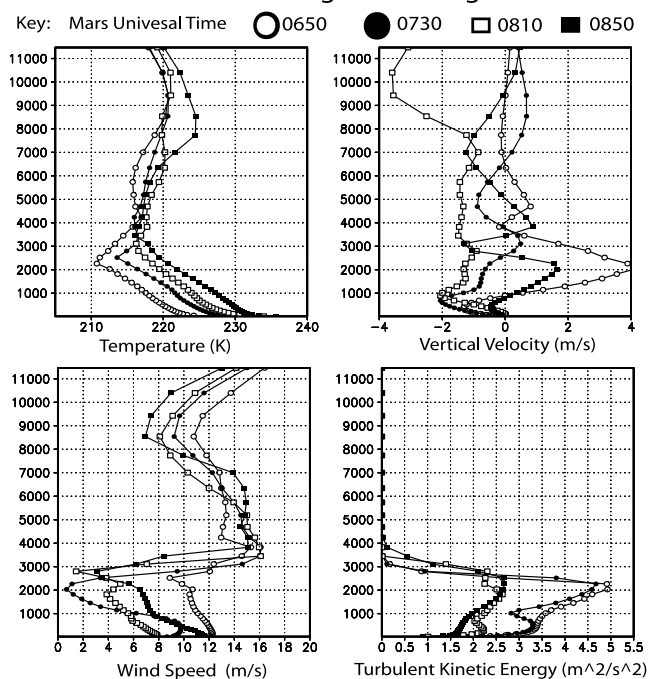


**Figure 2.** MRAMS timeseries of meteorological parameters for several sols at the beginning (solid) and end (dashed) of the mission. Time is given in Mars Universal Time (see text for description).

speed, which depends on what element of the organized structure within the PBL is over the site (see Section 3.2.3). The temperature field shows a superadiabatic lapse rate within the PBL, which is consistent with *Michaels and Rafkin* [2003]. The wind speed is relatively uniform and



**Figure 1.** MGCM timeseries of pressure, wind speed, and temperature for the duration of the primary mission. There are 16 data per sol.



**Figure 3.** Vertical profiles of meteorological parameters predicted by MRAMS during the EDL window. Time is in Mars Universal Time (add 6 hours to obtain local time).
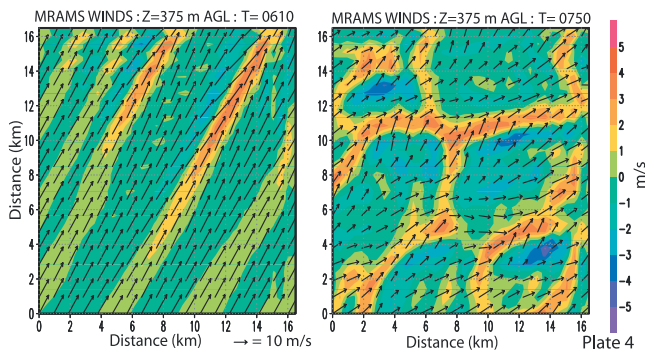
**Figure 4.** Vertical velocity (shaded) and winds (vectors) from the 6th grid of an MRAMS circulation. A benchmark wind vector length corresponding to 10 m/s is shown in the lower portion of the figure. The PBL structure evolves from linear updraft features (left) to polygonal updrafts (right). The structures move from northwest to southeast with the mean PBL wind. Only a portion of the grid domain is shown for clarity.

under 15 ms$^{-1}$ in the PBL. This is typical of a well-mixed atmospheric layer. A jet is found just above the PBL. Hence, a narrow region of wind shear marks the transition from the free atmosphere into the PBL.

[14] The vertical velocity field is highly variable, and the lower level structure is strongly dependent on the instantaneous structure of the PBL. Oscillations with a wavelength of approximately 1 km to 5 km are apparent above the PBL. These gravity waves are ubiquitous, and are triggered by the penetration of convective plumes into the stably stratified free atmosphere.

### 3.2.3. Structure of the Evolving Planetary Boundary Layer

[15] Figure 4 shows the evolution of the convective boundary layer. The evolution is consistent with that described by *Rafkin et al.* [2001, 2003], and *Michaels and Rafkin* [2003]. After sunrise, the nocturnal radiation inversion is quickly eroded. Then, horizontal rolls aligned with the mean wind shear vector develop with organized thermal plumes coincident with roll circulation convergence boundaries. These linear updraft structures move with the mean wind over the depth of the PBL.

[16] As radiative heating increases, the linear structures become curvilinear and intersect. In the later half of the afternoon, the intersecting lines of updrafts form polygons (usually hexagons), although they are slightly distorted by the wind in the downwind direction. The updrafts are narrow and intense in the lower half of the PBL, but weaken and widen near the top. Air subsides in the center of the polygons. The polygonal structures move with the mean wind.

[17] Throughout the afternoon, a point within the landing ellipse will experience the passage of dozens of these convective structures. Since the PBL is dominated by downdrafts on an area-weighted basis, it is likely that the lander will descend through a rather benign vertical velocity environment with magnitudes of about 1 ms$^{-1}$. However, it is possible that the lander could descend into or pass through a convective updraft, with vertical velocities of 10 ms$^{-1}$ or greater. There is also localized horizontal wind

shear that feeds the updraft at low levels. A vertical cross-section through these updrafts is shown in Figure 5.

### 3.2.4. Daily Weather

[18] The topography of Isidis Basin is very flat except for the occasional crater. Also, owing to its tropical location, it is not strongly influenced by middle latitude storm systems. Therefore, the weather in the central regions of the basin is controlled by daily, repeatable, large-scale atmospheric circulations, such as the tide, which are then modulated by the regional-scale circulations driven by the basin itself.

[19] Low-level winds at various times throughout a sol at the start and end of the mission are shown in Figure 6. Although the time series of meteorological parameters are very similar for the start and end of the mission (Figure 2), the basin-scale circulations are at times quite different.

[20] There is northeasterly large-scale flow directly into the basin at the start of the mission that interacts with the regional and local circulations. Near the time of sunrise (2230), downslope flows from the higher terrain have nearly reached the center of the basin. Weak large-scale flow into the basin is also evident. By mid-morning (0430), downslope winds and the large-scale circulation meet and produce a cyclonic circulation centered very near the landing site. Wind speeds are near their maximum at this time. As solar heating progresses, the winds turn to an upslope direction and the cyclonic circulation weakens. By late afternoon (1030), air enters at the northeast mouth of the basin and flows toward the higher topography. A secondary peak in wind speeds is present at this time, because the upslope winds are most fully developed, and the regional winds are reinforced by the large-scale flow. After sunset, the upslope winds begin to weaken, and only the large-scale flow into the basin remains. Downslope winds are reestablished in the early morning.

[21] In contrast to the start of the mission, the large-scale flow at the end of the mission is out of the basin. The circulation within the basin still exhibits a pronounced upslope/downslope flow during the day/night, but it does not interact with the large-scale circulation to produce the cyclonic structure seen at the start of the mission. Instead, the nighttime and morning downslope flows effectively flush the basin with the help of the larger-scale winds. The narrow opening in the northeast of the basin accelerates
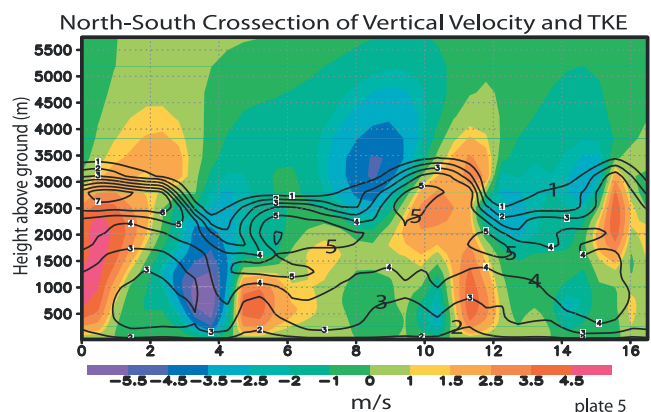


**Figure 5.** A vertical cross-section through the convective PBL during EDL. Vertical velocity is shaded, and TKE (m$^2$/s$^{-2}$) is contoured. See text for details.
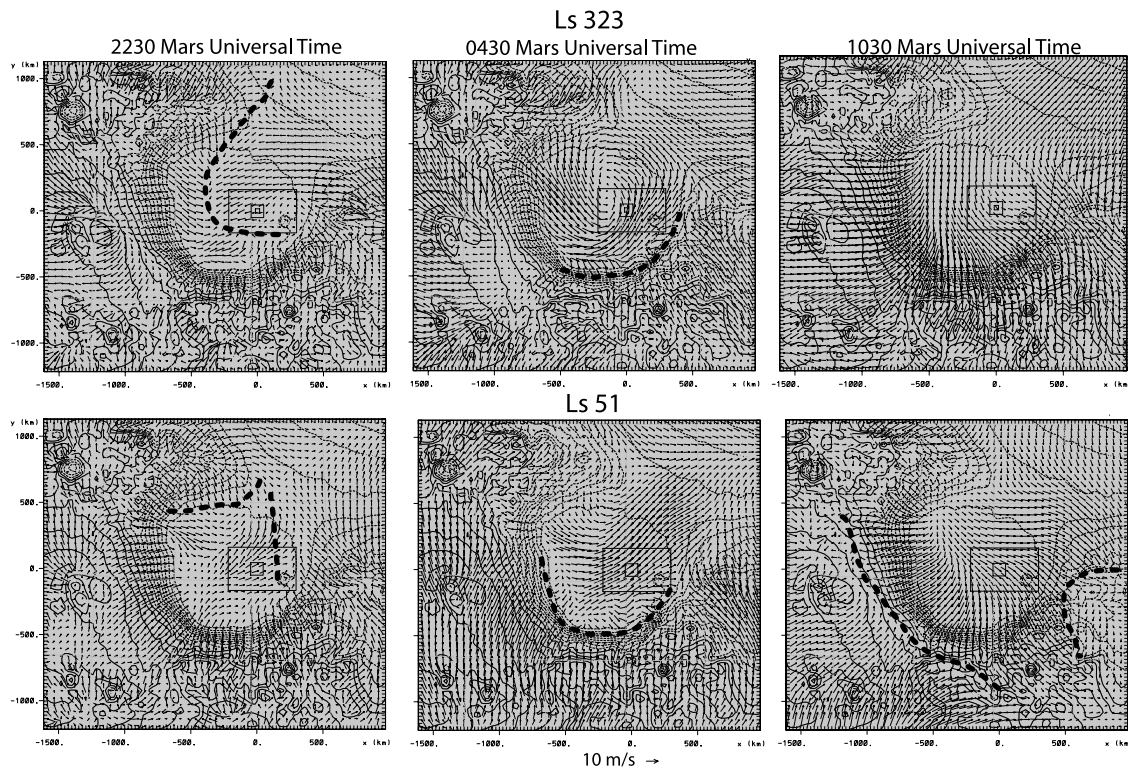
**Figure 6.** Horizontal cross-sections of winds (vectors) for the start and end of the mission at three different times during a sol. Topography is contoured. Convergence boundaries are indicated with a thick dashed line. Wind data are at ∼15 m above ground. See text for additional details.

these flushing winds. Otherwise, the circulations within the basin are outwardly similar to those at the start of the mission.

[22] The movement and penetration of the regional slope flows are influenced by the large-scale wind. For example, note that the upslope flows penetrate well into the southern highlands at 1030 at $L_s \approx 323$, aided by the large-scale northeasterly winds. This same upslope flow is opposed by the large-scale wind at $L_s \approx 51$, and the convergence boundary is very near the rim of the basin. Similarly, note the increased penetration of the downslope boundary at 2230 at $L_s \approx 51$ compared to $L_s \approx 323$.

## 4. Summary

[23] The MGCM and MRAMS models predict highly repeatable and relatively benign weather for the duration of the Beagle 2 primary mission. This is somewhat expected due to the tropical latitude and flat topography of the landing site. Large-scale near-surface wind speed never exceeds 15 ms$^{-1}$. Winds at the height of the Beagle 2 wind sensor should be less than those predicted by the MGCM and MRAMS due to its proximity to the surface. The models predict very little change in the daily temperature cycle. Some changes in the details of the daily pressure cycle are expected.

[24] The vertical wind structure at EDL is fairly benign except for strong wind shear at the top of the PBL, and strong vertical air currents associated with convective motions.

[25] Changes in the large-scale circulation modulate the underlying upslope/downslope mesoscale circulations. At the start of the mission the large-scale flow is directed into the basin from the northern lowlands. A cyclonic circulation within the basin develops as a consequence of this large-scale flow. Also, the daytime upslope flow on the south side of Isidis is enhanced, and it penetrates deeply into the southern highlands. At the end of the mission, the large-scale circulation is directed out of the basin. This allows the downslope flows to effectively flush the basin at night, and prevents the upslope flows along the southern flanks of the basin from penetrating into the highlands.

[26] The meteorological observations from Beagle 2 should be sufficient to assess the accuracy of surface meteorological predictions from the models. It is important that future missions continue to measure meteorological parameters whenever possible for the benefit of the missions that follow. The collected data are used to validate and improve the models, which will allow for more accurate atmospheric hazard assessment.

## References

Bridges, J. C., A. M. Seabrook, D. A. Rothery, J. R. Kim, C. T. Pilinger, M. R. Sims, M. P. Golembek, T. Duxbury, J. W. Head, A. F. C. Haldemann, K. L. Mitchell, J.-P. Muller, S. R. Lewis, C. Moncrieff, I. P. Wright, M. M. Grady, and J. G. Morley (2003), Selection of the landing site in Isidis Planitia of Mars Probe Beagle 2, *J. Geophys. Res.*, doi:10.1029/2001JE001820.

Haberle, R. M., J. R. Barnes, J. R. Murphy, M. M. Joshi, and J. Schaeffer (1997), Meteorological predictions for the Mars Pathfinder lander, *J. Geophys. Res.*, *102*, 13,301–13,311.

Kass, D. M., J. T. Schofield, T. I. Michaels, S. C. R. Rafkin, M. I. Richardson, and A. D. Toigo (2003), Analysis of atmospheric mesoscale models for entry, descent and landing, *J. Geophys. Res.*, in press.

Michaels, T. I., and S. C. R. Rafkin (2003), Large eddy simulation of atmospheric convection on Mars, Accepted, *Q. Journ. R. Meteorol. Soc.*

Rafkin, S. C. R., R. M. Haberle, and T. I. Michaels (2001), The Mars Regional Atmospheric Modeling System (MRAMS) Model description and selected simulations, *Icarus, 151*, 228–256.

Rafkin, S. C. R., and T. I. Michaels (2003), Meteorological Predictions for 2003 Mars Exploration Rover high-priority landing sites, *J. Geophys. Res.*, in press.

Toigo, A. D., and M. I. Richardson (2002), A mesoscale model for the Martian Atmosphere, *J. Geophys. Res., 107*, doi:10.1029/2000JE001489.

Toigo, et al. (2004), The Meteorology of proposed Mars Exploration Landing Sites, *J. Geophys. Res*, in press.

Tyler, D., J. R. Barnes, and R. M. Haberle (2002), Simulation of surface meteorology at the Pathfinder and VL1 sites using a Mars mesoscale model, *J. Geophys. Res.*, doi:10.1029/2001JE001618.

―――――――――

T. I. Michaels and S. C. R. Rafkin, Department of Space Studies, Southwest Research Institute, 1050 Walnut Street, suite 400, Boulder, CO 80302, USA. (srafkin@boulder.swri.edu)

R. M. Haberle, Space Science Division, NASA Ames Research Center, MS-245-3, Moffett Field, CA 94035, USA.